AD-A272 243

ICASE

20
Years of
Excellence

INVISCID INSTABILITY OF STREAMWISE
CORNER FLOW

DTIC
S ELECTE
NOV 10 1993
A

S. Balachandar

M. R. Malik

93-27650

ICASE Fluid Mechanics

Due to increasing research being conducted at ICASE in the field of fluid mechanics, future ICASE reports in this area of research will be printed with a green cover. Applied and numerical mathematics reports will have the familiar blue cover, while computer science reports will have yellow covers. In all other aspects the reports will remain the same; in particular, they will continue to be submitted to the appropriate journals or conferences for formal publication.

DTIC QUALITY INSPECTED 5

Accesion For		
NTIS CRA&I		Ⅵ
DTIC TAB		☐
Unannounced		☐
Justification		
By		
Distribution /		
Availability Codes		
Dist	Avail and / or Special	
A-1		

INVISCID INSTABILITY OF STREAMWISE CORNER FLOW

S. BALACHANDAR[1]

DEPARTMENT OF THEORETICAL AND APPLIED MECHANICS

UNIVERSITY OF ILLINOIS

URBANA, IL 61801

M.R. MALIK[1]

HIGH TECHNOLOGY CORPORATION

28 RESEARCH DRIVE

P.O. BOX 7262

HAMPTON, VA 23666

Abstract

Linear stability of the incompressible flow along a streamwise corner is studied by solving the two-dimensional eigenvalue problem governed by partial differential equations. It is found that this fully three-dimensional flow is subject to inviscid instability due to the inflectional nature of the streamwise velocity profile. The higher growth rates for the inviscid instability mode, which is symmetric about the corner bisector, as compared to the viscous Tollmien-Schlichting instability operative away from the corner is consistent with the experimental findings that the corner flow transitions to turbulence earlier than the two-dimensional Blasius flow away from the corner.

iii

1. INTRODUCTION

The last three decades saw significant progress towards better understanding of the stability of flow over two-dimensional and swept wing flows. These advancements have greatly improved our prediction and control capabilities of the laminar-turbulent transition process. For further progress it is important to enhance our understanding of the effects of geometric complications such as wing-body junction, finite wing span, and surface roughness elements, which play an important role in the overall transition process. Here we consider the inviscid stability of the flow along a streamwise corner, which can be considered as a model for the flow near a wing-body junction. The instability mechanisms induced by the streamwise corner will also help in assessing the effect of side walls on transitional and turbulent wind tunnel experiments. Understanding of the instability will also help us devise techniques for controlling transition in the corner flow.

The viscous flow along a corner that is formed by the intersection of two semi-infinite perpendicular plates (figure 1) is three dimensional close to the corner due to the strong interaction of the boundary layers on the two perpendicular walls. The basic laminar flow permits a similarity solution under boundary layer assumption. The governing self-similar boundary layer equations appropriate for the corner region, which blends with the two-dimensional Blasius boundary layer and the outer potential flow away from the cornerline, was obtained by Rubin (1966). Numerical solutions to these governing equations (Rubin & Grossman 1971 and Ghia 1975) exhibit a secondary cross-stream flow which is directed towards the corner along the two walls and directed away from the corner along the corner bisector. The resulting streamwise velocity profile along the corner bisector is inflectional in nature. Therefore the three-dimensional boundary layer near a streamwise corner is susceptible to inviscid instability, while the two-dimensional Blasius counterpart is only subjected to milder viscous instability.

Experiments on corner layer by Nomura (1962), Barclay (1973), El-Gamal & Barclay (1978) and Zamir & Young (1970, 1979) have yielded contrasting results for the laminar self-similar velocity profile. The differences among these experimental results highlight the exceptional sensitivity of the laminar corner layer solution to differences in the shape of the leading edge and streamwise pressure gradients (see Zamir 1981). This sensitivity to measurements can be attributed to the

1

early instability of the corner layer compared to the Blasius boundary layer. Based on his favourable pressure gradient experiments, Zamir (1981) observes that the zero pressure gradient corner layer becomes unstable at a Reynolds number of around 10^4, while the critical Reynolds number for a zero pressure gradient flat plate boundary layer is an order of magnitude higher, around 10^5.

Lakin & Hussaini (1984) considered the stability of the corner flow sufficiently away from the cornerline in the blending region, where the streamwise and wall normal velocities are given by the Blasius solution with a superimposed secondary spanwise velocity induced by the corner. Solutions to the stability equations were obtained with a critical layer analysis. Recently, Dhanak (1993) studied the stability of the blending boundary layer numerically, employing the same governing equations as those of Lakin & hussaini but emphasized the importance of enforcing appropriate symmetry boundary conditions along the corner bisector, instead of the usual asymptotic boundary conditions at infinity for the one-dimensional problem. However, his results close to the corner region are quantitatively questionable since the one-dimensional stability analysis employed in his analysis ignores any spanwise variation of the mean flow. Where as the actual flow is three dimensional close to the corner and the approach towards the Blasius boundary layer is only algebraic (Pal & Rubin 1971).

Here we will retain the strong dependence of the corner boundary layer along the two wall normal directions and consider the stability of this flow with a locally parallel assumption along the streamwise direction. The resulting two-dimensional stability analysis results in an eigenvalue problems which poses far greater computational challenges than the one-dimensional counterpart. To simplify the analysis and computations, we will restrict attention to an inviscid analysis through an extended Rayleigh equation (a partial differential equation). The inviscid analysis should be adequate to capture the qualitative features of the dominant instability mechanism arising from the inflectional nature of the streamwise velocity component.

2. Mathematical Formulation

2.1 Mean Flow

The viscous flow along the corner that is formed by the intersection of two semi-infinite perpendicular flat plates (Figure 1) can be simplified with the boundary layer theory. Unlike flat plate

and infinite wing geometries, the corner flow is three-dimensional (all three velocity components exist and they are function of all three coordinates). Sufficiently far way from both the flat plates (region I) the flow can be modelled as potential flow. Close to the plates but far away from the corner line (regions II and III) the mean flow is nearly two-dimensional and depends only on x and y coordinates in region II and on x and z coordinates in region III. These two-dimensional blending boundary layers are primarily Blasius boundary layers, but with a superposed transverse flow. In the region close to the corner line (region IV) the coupling that is created by the mutual interaction results in a strongly three dimensional boundary layer. The flow in this corner region, termed as the "corner layer" is the subject matter of this paper.

The governing three-dimensional boundary layer equations appropriate within the corner layer can be written in a self-similar form as follows (Rubin 1966):

$$-\eta\frac{\partial\hat{u}}{\partial\eta} - \zeta\frac{\partial\hat{u}}{\partial\zeta} + \frac{\partial\hat{v}}{\partial\eta} + \frac{\partial\hat{w}}{\partial\zeta} = 0 \tag{1.1}$$

$$-\eta\,\hat{u}\frac{\partial\hat{u}}{\partial\eta} - \zeta\,\hat{u}\frac{\partial\hat{u}}{\partial\zeta} + \hat{v}\frac{\partial\hat{u}}{\partial\eta} + \hat{w}\frac{\partial\hat{u}}{\partial\zeta} = \frac{\partial^2\hat{u}}{\partial\eta^2} + \frac{\partial^2\hat{u}}{\partial\zeta^2} \tag{1.2}$$

$$-\hat{u}\,\hat{v} - \eta\,\hat{u}\frac{\partial\hat{v}}{\partial\eta} - \zeta\,\hat{u}\frac{\partial\hat{v}}{\partial\zeta} + \hat{v}\frac{\partial\hat{v}}{\partial\eta} + \hat{w}\frac{\partial\hat{v}}{\partial\zeta} = -\frac{\partial\hat{p}}{\partial\eta} + \frac{\partial^2\hat{v}}{\partial\eta^2} + \frac{\partial^2\hat{v}}{\partial\zeta^2} \tag{1.3}$$

$$-\hat{u}\,\hat{w} - \eta\,\hat{u}\frac{\partial\hat{w}}{\partial\eta} - \zeta\,\hat{u}\frac{\partial\hat{w}}{\partial\zeta} + \hat{v}\frac{\partial\hat{w}}{\partial\eta} + \hat{w}\frac{\partial\hat{w}}{\partial\zeta} = -\frac{\partial\hat{p}}{\partial\zeta} + \frac{\partial^2\hat{w}}{\partial\eta^2} + \frac{\partial^2\hat{w}}{\partial\zeta^2} \tag{1.4}$$

where η and ζ are the nondimensional boundary layer coordinates along the wall normal directions y and z given by

$$\eta = \frac{y}{\sqrt{2}x^*}\mathrm{Re}^{1/2} \qquad \text{and} \qquad \zeta = \frac{z}{\sqrt{2}x^*}\mathrm{Re}^{1/2} \tag{2}$$

where the Reynolds number is defined as $\mathrm{Re} = \frac{Ux^*}{\nu}$. The dependent variables $\hat{u}$, $\hat{v}$, $\hat{w}$ and $\hat{p}$ are the nondimensional velocity components and pressure and are related to their dimensional values u, v and w and p through the following relations:

$$\hat{u} = \frac{u}{U}, \qquad \hat{v} = \frac{\sqrt{2}v}{U}\mathrm{Re}^{1/2}, \qquad \hat{w} = \frac{\sqrt{2}w}{U}\mathrm{Re}^{1/2}, \qquad \hat{p} = \frac{2p}{\varrho\,U^2}\mathrm{Re} \ . \tag{3}$$

Here U is the free stream velocity, x^* is the dimensional distance from the leading edge, ϱ and ν are the density and kinematic viscosity of the fluid. The dependence on the streamwise direction, x, has

3

been eliminated in the above equation (1) by assuming a self similar solution for the corner layer along the streamwise direction.

The elliptic nature of the governing equation (1) requires boundary conditions for $\hat{u}$, $\hat{v}$, $\hat{w}$ on the four bounding lines; $\eta = 0$, $\zeta = 0$, $\eta = \eta_{max} \to \infty$, $\zeta = \zeta_{max} \to \infty$. The proper boundary conditions on the two walls are no-slip and no-penetration. The asymptotic boundary conditions appropriate in the limit of $\zeta_{max} \to \infty$, and $\eta < \zeta$, should blend with the blending boundary layer (region II). By symmetry the same boundary condition applies in the limit of $\zeta_{max} \to \infty$. These asymptotic boundary conditions can be expressed as the following expansion in inverse powers of distance from the cornerline (Pal & Rubin 1971)

$$\hat{u}(\eta,\zeta_{max}) = \hat{u}_0(\eta) + \frac{\hat{u}_1(\eta)}{\zeta_{max}} + \frac{\hat{u}_2(\eta)}{\zeta_{max}^2} + \frac{\hat{u}_3(\eta)}{\zeta_{max}^3} \tag{4.1}$$

$$\hat{v}(\eta,\zeta_{max}) = \hat{v}_0(\eta) + \frac{\hat{v}_1(\eta)}{\zeta_{max}} + \frac{\hat{v}_2(\eta)}{\zeta_{max}^2} + \frac{\hat{v}_3(\eta)}{\zeta_{max}^3} \tag{4.2}$$

$$\hat{w}(\eta,\zeta_{max}) = \hat{w}_1(\eta) + \frac{\hat{w}_2(\eta)}{\zeta_{max}} + \frac{\hat{w}_3(\eta)}{\zeta_{max}^2} \tag{4.3}$$

$$\hat{p}(\eta,\zeta_{max}) = \hat{p}_0(\eta) + \frac{\hat{p}_1(\eta)}{\zeta_{max}} + \frac{\hat{p}_2(\eta)}{\zeta_{max}^2} + \frac{\hat{p}_3(\eta)}{\zeta_{max}^3} \tag{4.4}$$

The zeroth order boundary conditions, $\hat{u}_0$, $\hat{v}_0$ and $\hat{p}_0$, are nothing but the Blasius boundary layer solutions. The first order streamwise and wall normal velocities can be shown to be zero (Pal & Rubin 1971) and the only first order effect of the corner is to induce the secondary flow, $\hat{w}_1$, towards the corner along the bottom wall. The higher order terms in the above equation have been obtained by Pal & Rubin (1971) by requiring a simultaneous matching of the corner layer with the outer potential flow as η, $\zeta \to \infty$. Thus the above equation (4) provides asymptotically accurate higher order boundary condition which can be applied at the outer boundaries of a computational domain that has been truncated to a large but finite $\eta = \eta_{max}$ and $\zeta = \zeta_{max}$. The above equation displays the algebraic decay towards the Blasius boundary layer as $\zeta \to \infty$.

The governing equation (1) can be solved with wall boundary conditions and asymptotic outer boundary conditions (equation 4) to obtain the laminar corner layer. This problem of obtaining the corner mean flow has been addressed by many authors (Carrrier 1947, Pearson 1957, Rubin &

Grossman 1971, Desai & Mangler 1974 and Ghia 1975) with varying degrees of approximations applied to the governing equations and the boundary conditions. Here we have employed a spectral ADI technique in order to solve the corner layer equations. The spectral discretization will provide exponential accuracy needed for accurate stability calculations. Results obtained from this technique compare favourably with those of Rubin & Grossman (1971) and Ghia (1975). Figure 2 shows contours of streamwise velocity and a vector plot of the cross-stream secondary velocity. Figure 3 shows the velocity profiles plotted along the corner bisector. An inflection point in the streamwise velocity profile at $\eta = \zeta \approx 2.4$ is evident.

3. Stability Analysis

The stability of the laminar base flow to small perturbations can be investigated through the standard linear stability analysis. By making a quasi-parallel flow assumption for the base flow along the streamwise direction, velocity and pressure perturbations of the following form (normal mode *anastaz*) can be superimposed on to the mean flow

$$u_p = \hat{u}_p(\eta,\zeta)\exp[\iota(a\xi - \omega t)] \qquad v_p = \hat{v}_p(\eta,\zeta)\exp[\iota(a\xi - \omega t)]$$
$$w_p = \hat{w}_p(\eta,\zeta)\exp[\iota(a\xi - \omega t)] \qquad p_p = \hat{p}_p(\eta,\zeta)\exp[\iota(a\xi - \omega t)] \tag{5}$$

where ξ is the non-dimensional streamwise coordinate and $\sqrt{2}x^*\mathrm{Re}^{-1/2}$ and U are used as the length and velocity scales. These perturbation quantities will be added to the nondimensionalized base flow ($\hat{u}_m = \hat{u}$, $\hat{v}_m = \hat{v}(2\,\mathrm{Re})^{-1/2}$, $\hat{w}_m = \hat{w}(2\,\mathrm{Re})^{-1/2}$) and the total velocity and pressure when substituted into the Navier-Stokes equation and the incompressibility condition and linearized results in the following stability equations

$$\hat{u}_m\,\iota\,a\,\hat{u}_p + \hat{v}_m\frac{\partial\hat{u}_p}{\partial\eta} + \hat{w}_m\frac{\partial\hat{u}_p}{\partial\zeta} + \hat{v}_p\frac{\partial\hat{u}_m}{\partial\eta} + \hat{w}_p\frac{\partial\hat{u}_m}{\partial\zeta} + \iota\,a\,\hat{p}_p - \frac{L}{R}\hat{u}_p = \iota\,\omega\,\hat{u}_p \tag{6.1}$$

$$\hat{u}_m\,\iota\,a\,\hat{v}_p + \hat{v}_m\frac{\partial\hat{v}_p}{\partial\eta} + \hat{w}_m\frac{\partial\hat{v}_p}{\partial\zeta} + \hat{v}_p\frac{\partial\hat{v}_m}{\partial\eta} + \hat{w}_p\frac{\partial\hat{v}_m}{\partial\zeta} + \frac{\partial\hat{p}_p}{\partial\eta} - \frac{L}{R}\hat{v}_p = \iota\,\omega\,\hat{v}_p \tag{6.2}$$

$$\hat{u}_m\,\iota\,a\,\hat{w}_p + \hat{v}_m\frac{\partial\hat{w}_p}{\partial\eta} + \hat{w}_m\frac{\partial\hat{w}_p}{\partial\zeta} + \hat{v}_p\frac{\partial\hat{w}_m}{\partial\eta} + \hat{w}_p\frac{\partial\hat{w}_m}{\partial\zeta} + \frac{\partial\hat{p}_p}{\partial\zeta} - \frac{L}{R}\hat{w}_p = \iota\,\omega\,\hat{w}_p \tag{6.3}$$

$$\iota\,a\,\hat{u}_p + \frac{\partial\hat{v}_p}{\partial\eta} + \frac{\partial\hat{w}_p}{\partial\zeta} = 0 \tag{6.4}$$

where operator $L = -a^2 + \frac{\partial^2}{\partial\eta^2} + \frac{\partial^2}{\partial\zeta^2}$ and $R = \sqrt{2\,\mathrm{Re}}$. In the above temporal stability formula-

tion, the input parameters to the stability analysis, α and Re, are respectively the streamwise wave-number and Reynolds number and ω is the resulting complex eigenvalue whose real part represents the disturbance frequency and the imaginary part corresponds to the disturbance growth rate. Hence if $\omega_{imag\_part} > 0$, corner flow is susceptible to unstable small amplitude disturbances.

3.1. Bisector Instability

Before solving the partial differential eigenvalue problem (equation 6), we will first consider the effect of the inflectional profile by studying the simpler problem of the one-dimensional stability of the velocity profile along the corner bisector. Instead of the cartesian coordinates η and ζ a new orthogonal coordinate system s and t will be considered, where s is along the corner bisector. In the transformed coordinates a locally parallel flow assumption is made by ignoring the variations in the mean flow along the streamwise ζ and tangential t directions and stability of this one-dimensional base flow to disturbances of the following form is considered

$$\begin{Bmatrix} \hat{u}_p(s) \\ \hat{v}_p(s) \\ \hat{w}_p(s) \\ \hat{p}_p(s) \end{Bmatrix} \exp[\iota(\alpha\xi + \beta t - \omega t)]$$

The results obtained from this bisector stability analysis will be presented below to provide qualitative understanding of the effect of the inflectional nature of the base flow on the overall stability. Figure 4 shows temporal growth rate (imaginary part of ω) of the disturbance plotted against streamwise wavenumber α at three different Reynolds numbers, Re=5000 (case I); Re=4.5×10^4 (case II) and Re=1.25×10^5 (case III). Two-dimensional disturbances corresponding to β=0 are the most amplified and results corresponding to this case only will be presented. The outer edge of the computational domain is chosen to be s_{max}=25 and is discretized by 85 Chebyshev Gauss–Lobatto points and asymptotic boundary conditions are applied at the outer edge. The results presented are well converged and show insensitivity to the exact number of grid points, location and nature of the outer boundary condition. Also plotted in figure 4 is growth rate vs $(Re)^{1/2}$ for α=0.21 (case IV). A critical Reynolds number of Re$_{crit}$=435.0 is obtained and the corresponding critical streamwise wavelength, α_{crit}=0.2 and the critical frequency, $(\omega_{crit})_{real\_part}$=0.1. This result compared with the critical Reynolds number of 9.1×10^4 for the Blasius profile shows that the inflection point induced by the

6

streamwise corner has the potential to decrease the critical Reynolds number by as much as two orders of magnitude. Owing to its inviscid nature, the growth rates for the bisector profile are also much larger than those of the Tollmien-Schlichting disturbance in the Blasius boundary layer. Figure 5 shows the frequency ($\omega_{\text{real\_part}}$) variation corresponding to the four cases discussed above. As expected the frequency varies linearly with a for large values of the wavenumber and is almost independent of the Reynolds number.

3. 2. The Two-Dimensional Inviscid Eigenvalue Problem

With the above encouraging results we will consider the two-dimensional inviscid instability of the corner flow in the limit of Re $\rightarrow \infty$. In this limit the viscous terms drops out of equation (6). It should also be noted that in the limit of infinite Reynolds number the mean flow is purely streamwise, since in the boundary layer approximation the cross-stream velocities, $\hat{v}_m$ and $\hat{w}_m$, are order $\frac{1}{\sqrt{\text{Re}}}$ smaller than the streamwise velocity. Equation (6) can therefore be simplified as:

$$- \iota\,\omega\,\hat{u}_p + \hat{u}_m\,\iota\,a\,\hat{u}_p + \hat{v}_p\frac{\partial\hat{u}_m}{\partial\eta} + \hat{w}_p\frac{\partial\hat{u}_m}{\partial\zeta} = -\iota\,a\,\hat{p}_p \tag{7.1}$$

$$- \iota\,\omega\,\hat{v}_p + \hat{u}_m\,\iota\,a\,\hat{v}_p = -\frac{\partial\hat{p}_p}{\partial\eta} \tag{7.2}$$

$$- \iota\,\omega\,\hat{w}_p + \hat{u}_m\,\iota\,a\,\hat{w}_p = -\frac{\partial\hat{p}_p}{\partial\zeta} \tag{7.3}$$

$$\iota\,a\,\hat{u}_p + \frac{\partial\hat{v}_p}{\partial\eta} + \frac{\partial\hat{w}_p}{\partial\zeta} = 0 \tag{7.4}$$

The above linear momentum and continuity equations can be combined to form the following single higher order equation for the pressure perturbation (Hall & Horseman 1990):

$$- a^2\,\hat{u}_m\,\hat{p}_p + \hat{u}_m\frac{\partial^2\hat{p}_p}{\partial\eta^2} - 2\frac{\partial\hat{u}_m}{\partial\eta}\frac{\partial\hat{p}_p}{\partial\eta} + \hat{u}_m\frac{\partial^2\hat{p}_p}{\partial\zeta^2} - 2\frac{\partial\hat{u}_m}{\partial\zeta}\frac{\partial\hat{p}_p}{\partial\zeta} = \frac{\omega}{a}\,L\hat{p}_p \tag{8}$$

We will employ a spectral methodology (Canuto *et al.* 1988) for solving the above eigenvalue problem with Chebyshev discretization along the η and ζ directions. With this spatial discretization equation (8) reduces to a generalized matrix eigenvalue problem of the form

$$\underline{\underline{A}}\,\hat{p}_p = \frac{\omega}{a}\underline{\underline{B}}\,\hat{p}_p \tag{9}$$

With N grid points along each of the η and ζ directions the size of the matrix eigenvalue problem

is nearly $N^2 \times N^2$, therefore computational time and memory places stringent limitations on the spatial resolution. Here we have employed the inviscid approximation since the discretized matrix for the viscous eigenvalue problem (Eqn. 6) is sixteen fold larger. The following symmetry conditions

$$
\begin{array}{cc}
\underline{\textbf{Symmetric Mode}} & \underline{\textbf{Anti-Symmetric Mode}} \\
\hat{u}_p(\eta,\zeta) = \hat{u}_p(\zeta,\eta) & \hat{u}_p(\eta,\zeta) = -\hat{u}_p(\zeta,\eta) \\
\hat{v}_p(\eta,\zeta) = \hat{w}_p(\zeta,\eta) & \hat{v}_p(\eta,\zeta) = -\hat{w}_p(\zeta,\eta) \\
\hat{p}_p(\eta,\zeta) = \hat{p}_p(\zeta,\eta) & \hat{p}_p(\eta,\zeta) = -\hat{p}_p(\zeta,\eta)
\end{array}
\qquad (10)
$$

can be used to reduce the size of the matrix four fold, but the eigenvalue problem still remains formidable.

In the inviscid limit the appropriate boundary condition to be applied on the solid boundaries for the velocity eigenfunctions is no penetration. From equations 7.2 and 7.3, the corresponding pressure boundary conditions on the solid boundaries are zero normal derivatives. The computational domain will be truncated to be a finite square and the outer boundary conditions will be imposed at $\eta = \eta_{max}$ and $\zeta = \zeta_{max}$. The appropriate boundary condition for pressure at these outer boundaries is not clear. But far away from the corner ($\eta = \eta_{max}$, $\zeta = \zeta_{max}$) the streamwise velocity profile is not inflectional and will not support inviscid instability. Therefore, it is reasonable to assume that $\hat{p}_p = 0$ at $\eta = \eta_{max}$ and $\zeta = \zeta_{max}$. In any case, the eigenvalue problem was solved with both Dirichlet ($\hat{p}_p = 0$) and Neumann $\left[\dfrac{\partial \hat{p}_p}{\partial \eta} = \dfrac{\partial \hat{p}_p}{\partial \zeta} = 0 \right]$ boundary conditions and the sensitivity of the stability results to the placement of the outer boundary at $\eta = \eta_{max}$ and $\zeta = \zeta_{max}$ and to the number of grid points was also considered. Based on these sensitivity tests $\eta_{max} = \zeta_{max} = 25$ with 55 Chebyshev Gauss–Lobatto points along both the η and ζ directions was found adequate to provide well converged results. Both Dirichlet and Neumann boundary conditions for pressure at the outer boundaries yielded identical results to 5 decimal places.

Only results for the symmetric disturbance case will be presented below. The anti-symmetric disturbances did not provide any growing solution. This result is to be expected since the symmetric disturbances have their peak value along the corner bisector, where the base flow is inflectional.

8

Whereas, the pressure and streamwise velocity components of the antisymmetric disturbance mode are zero along the corner bisector. Although, there are no growing anti-symmetric modes in the inviscid limit, we anticipate growing anti-symmetric (Tollmien-Schlichting like) viscous modes in a full viscous stability problem, but their growth rate will still be smaller than the corresponding symmetric inviscid mode.

In figure 6 the growth rate of the most unstable inviscid instability mode is plotted as a function of the streamwise wave number. The continuous curve corresponds to the case where homogeneous Dirichlet condition is used at the outer boundaries for the pressure eigenfunction and the symbols correspond to the case of homogeneous Neumann pressure boundary condition. Insensitivity of the results to the exact nature of the boundary condition is apparent, indicating that $\eta_{max} = \zeta_{max} = 25$ is adequately away from the corner region. Also plotten in this figure is the growth rate of the second most unstable mode, whose maximum growth rate is nearly two and a half times smaller than that of the most unstable mode. The corresponding frequency variations are shown in figure 7 as a function of the streamwise wavenumber. A nearly linear increase in frequency with wavenumber can be observed. The frequency corresponding to the second most unstable mode is slightly smaller than that of the most unstable mode.

The inviscid instability mode with the largest growth rate corresponds to a streamwise wavenumber of $\alpha=0.225$. This result compares well with results obtained from the bisector instability analysis, where α corresponding to the most amplified disturbance is 0.20 at Re=5000 and 0.21 at Re=4.5×10^4 and further increases with Reynolds number. The maximum growth rate (imaginary part of ω) obtained from the two-dimensional inviscid instability analysis is 0.004 and is much smaller than those obtained from the one-dimensional bisector instability analysis. This is because the mean flow in the two-dimensional analysis progressively becomes less inflectional away from the corner bisector and the overall effect is to reduce the growth rate in comparison with the one-dimensional analysis. The frequency (real part of ω) obtained from these two instability analysis agrees very well. For example, the non-dimensional frequency of the most amplified two-dimensional inviscid mode is 0.1 which compares well with $(\omega)_{real\_part}=0.089$ and 0.092 for the most amplified bisector modes at Re= 5000 and 4.5×10^4 , respectively.

9

Figures 8a and 8b show the real and imaginary parts of the most amplified pressure eigenfunction ($\alpha = 0.225$; $\omega = 0.108 + \iota\, 0.003975$). Peak values of the real part of the pressure eigenfunction occurs along the corner bisector near $\eta = \zeta = 2.5$ where the mean streamwise velocity profile is inflectional. Although the peak values of the imaginary part occur away from the corner bisector closer to the walls, the magnitude of the real part dominates the imaginary part. From the pressure eigenfunctions the corresponding velocity eigenfunctions can be evaluated based on equation (7). Figures 9a and 9b show contours of the v-eigenfunction plotted in two different ranges. It is clear from this figure that the v–velocity of the disturbance rapidly increases near the critical layer where the denominator $\iota(\alpha \hat{u}_m - \omega)$ that occurs in the evaluation of the velocity eigenfunctions become nearly singular. But the pressure eigenfunction is well behaved in this critical layer region and therefore the eigenvalue computations are well resolved. The corresponding w-eigenfunctions can be obtained from figure 9 based on the even parity of the w and v eigenfunctions about the corner bisector.

4. Conclusions

Finally we conclude with a few comments on how the above results are relevant in explaining the rapid transition observed in zero pressure gradient corner flow experiments. The two-dimensional inviscid instability analysis, although confirms the possibility of an inviscid instability due to the inflectional nature of the mean streamwise velocity does not provide any clue as to the critical Reynolds number for this mechanism to be active. On the other hand, the bisector instability analysis, although it ignores all variations in the mean flow away from the bisector, yields a critical Reynolds number of 435. In any case, these results suggest a possible destabilizing inviscid mechanism active starting from a point close to the leading edge as compared to the corresponding viscous instability in the Blasius boundary layer. These results are consistent with the experimental observations of Zamir (1981) that the corner flow becomes transitional at Reynolds numbers $\approx 10^4$ compared with the critical Reynolds number of $\approx 9 \times 10^4$ for the Blasius boundary layer. Further confirmation of the present results with a full two-dimensional viscous stability analysis (using equation (6)) is currently being pursued.

REFERENCES

Barclay, W.H. *Aeronaut. Q.*, **24**, 147, 1973.

Canuto, C., Hussaini, M.Y., Quarteroni, A. and Zang, T.A. *Spectral Methods in Fluid Dynamics*, Springer-Verlag, New York, 1988.

Carrier, G., The boundary layer in a corner, *Quart. Appl. Math*, **4**, 367, 1947.

Desai, S.S. and Mangler, K.W., Incompressible laminar boundary layer flow along a corner formed by two intersecting planes, *Royal Aircraft Establishment*, **TR 74062**, 1974.

Dhanak, M.R., On the instability of flow in a streamwise corner, *Proc. R. Soc. Lond. A*, **441**, 201, 1993.

El-Gamal, H.A. and Barclay, W.H., *Aeronaut. Q.* **29**, 75, 1978

Ghia, K.N., Incompressible streamwise flow along an unbounded corner, *AIAA J.*, **13**, 902, 1975.

Hall, P., and Horseman, N.J., The inviscid secondary instability of fully nonlinear longitudinal vortex structures in growing boundary layers, *ICASE Report*, **90-71**, 1990.

Lakin, W.D., and Hussaini, M.Y., Stability of the laminar boundary layer in a streamwise corner, *Proc. R. Soc. Lond. A*, **393**, 101, 1984.

Nomura, Y., *Mem. Def. Acad. Math. Phys. Chem. Engng., Yokosuka, Japan*, **22**, 115, 1962.

Pal. A. and Rubin, S.G., Asymptotic features of the viscous flow along a corner, *Quart. Appl. Math.*, **29**, 91, 1971.

Pearson, J.R.A., Homogeneous turbulence and laminar viscous flow, *Ph.D. Thesis*, Cambridge University, 1957.

Rubin, S.G., Incompressible flow along a corner, *J. Fluid Mech.*, **26**, 97, 1966.

Rubin, S.G. and Grossman, B., Viscous flow along a corner: numerical solution of the corner layer equations, *Quart. Appl. Math.*, **24**, 169, 1971.

Zamir, M. and Young, A.D., *Aeronaut. Q.*, **21**, 313, 1970

Zamir, M. and Young, A.D., *Aeronaut. Q.*, **30**, 471, 1979

Zamir, M., Similarity and stability of the laminar boundary layer in a streamwise corner, *Proc. R. Soc. Lond. A*, **377**, 269, 1981.

Figure Captions

Figure 1: Streamwise corner flow geometry and the coordinate system used.

Figure 2: Contour plot of the streamwise component of the mean velocity field. There are 19 contour lines running from 0.05 near the walls to 0.95 away from the walls. Also shown is a vector plot of the cross-stream velocity components.

Figure 3: Velocity components along the streamwise direction and along the corner bisector plotted against distance from the cornerline along the corner bisector (s). Due to boundary layer scaling the actual velocity component along the corner bisector is order $(Re)^{1/2}$ smaller than the streamwise component.

Figure 4: Growth rate obtained from the bisector instability analysis. Case I: growth rate vs a for Re=5000; case II: growth rate vs a for Re=4.5×10^4; case III: growth rate vs a for Re=1.25×10^5; case IV: growth rate vs Re for a=0.21.

Figure 5: Frequency obtained from the bisector instability analysis. Case I: Frequency vs a for Re=5000; case II: Frequency vs a for Re=4.5×10^4; case III: Frequency vs a for Re=1.25×10^5; case IV: Frequency vs Re for a=0.21.

Figure 6: Growth rate vs a obtained from the inviscid instability analysis for the first two most unstable disturbance modes. Slid line corresponds to the most unstable mode and the dashed line corresponds to the second most unstable mode.

Figure 7: Frequency vs a obtained from the inviscid instability analysis for the first two most unstable disturbance modes. Slid line corresponds to the most unstable mode and the dashed line corresponds to the second most unstable mode.

Figure 8: Contours of the real (a) and the imaginary (b) parts of the pressure eigenfunction corresponding to the most amplified inviscid disturbance. For the real part there are 21 contour lines ranging from -1.0 (marked 1) to 0.0 (marked L) and for the imaginary part there are 21 contours ranging from -0.2 (marked 1) to 0.1 (marked L).

Figure 9: Contours of the absolute value of the v-velocity eigenfunction corresponding to the most amplified inviscid disturbance. For clarity the contours are plotted in two different ranges. In figure 9a there are 19 contours ranging from 1.0 (marked 1) to 19.0 (marked J) and in figure 9b there are 20 contours ranging from 0.1 (marked 1) to 2.0 (marked K).
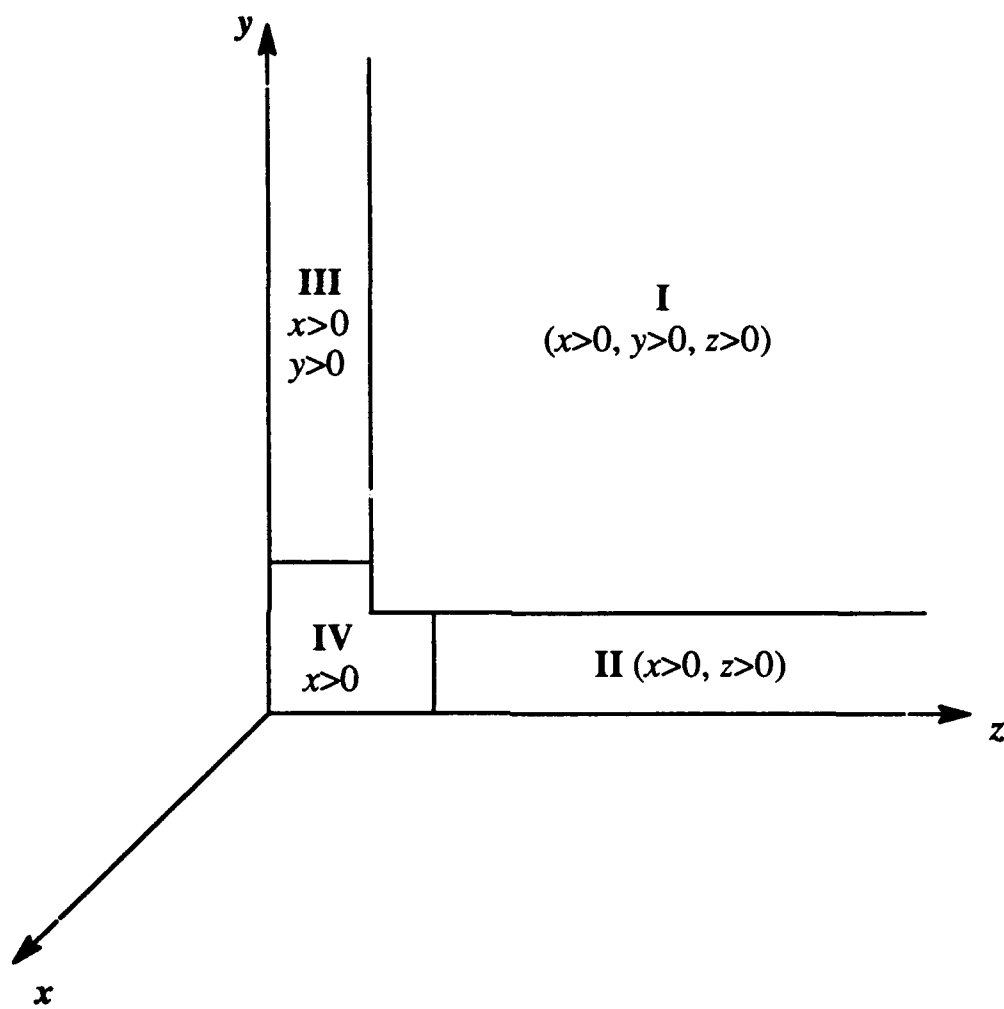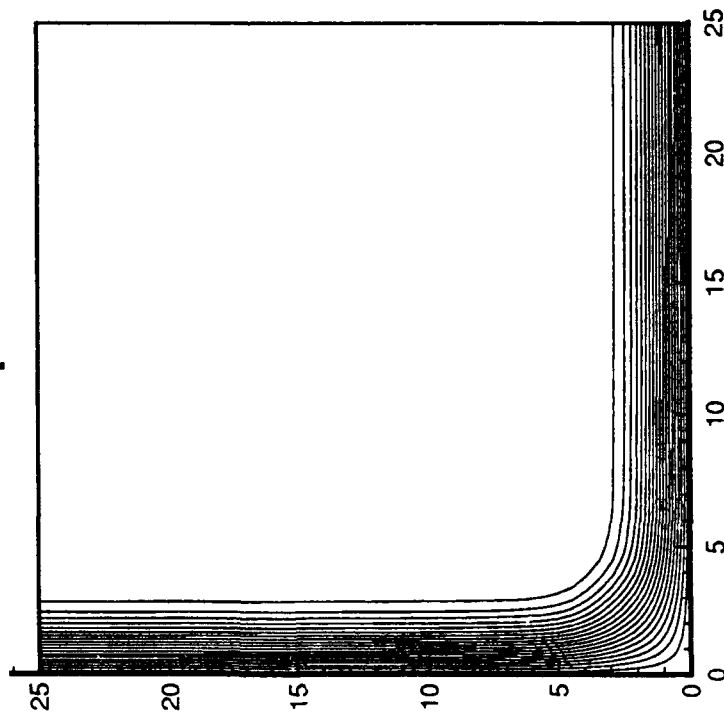
Figure 1: Corner Flow geometry

Cross-Stream Velocity Vector Plot

Streamwise Component of Mean Flow
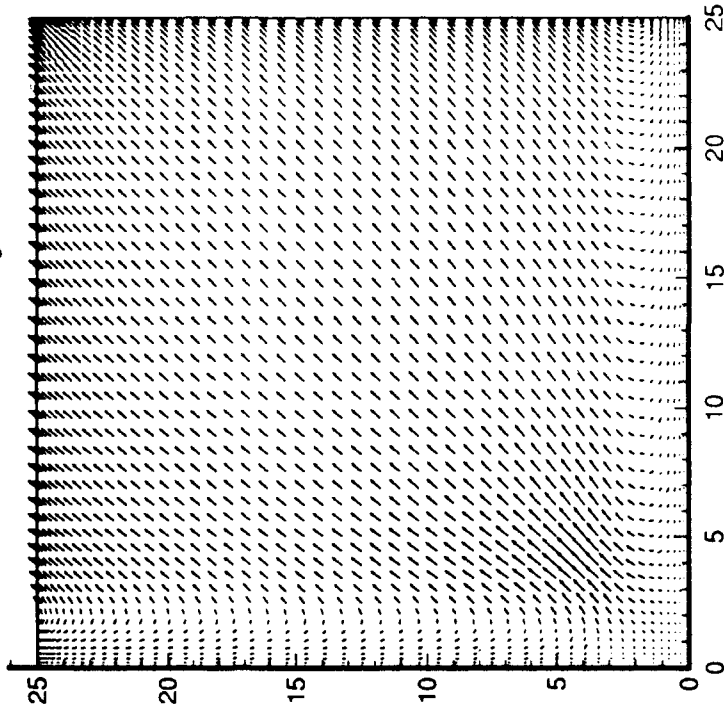
Figure 2

14

Figure 3

$v_s (Re)^{1/2}$

u
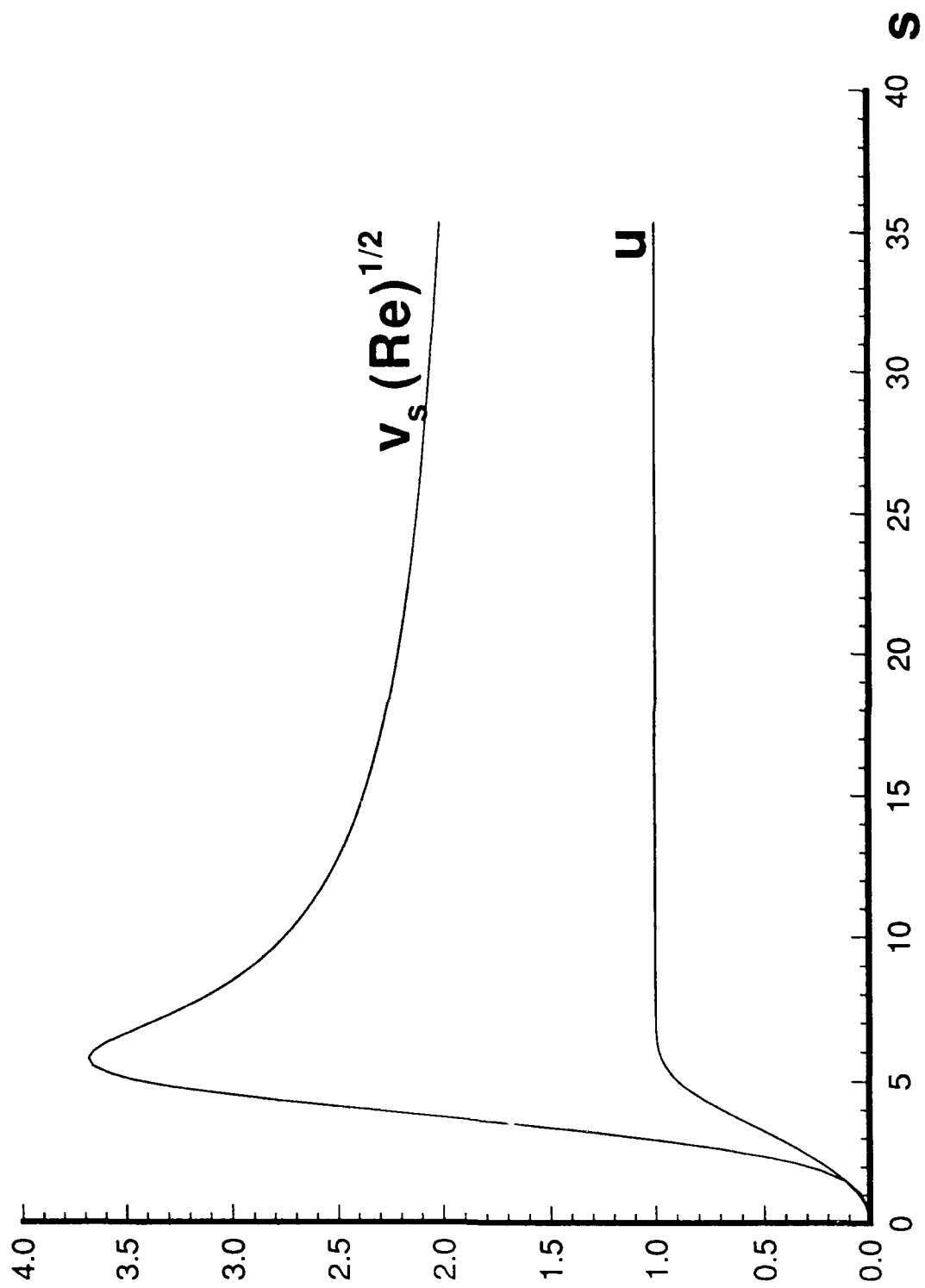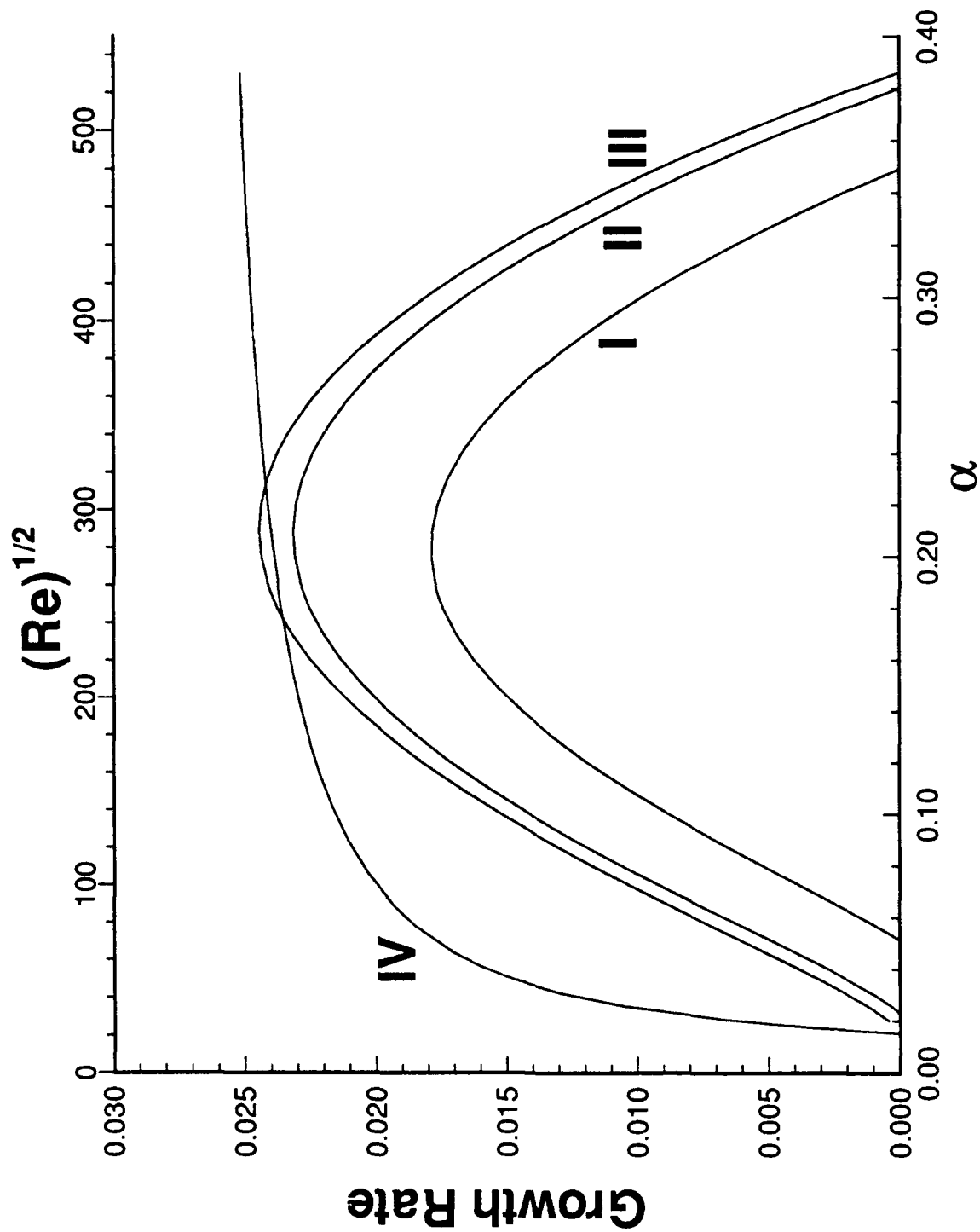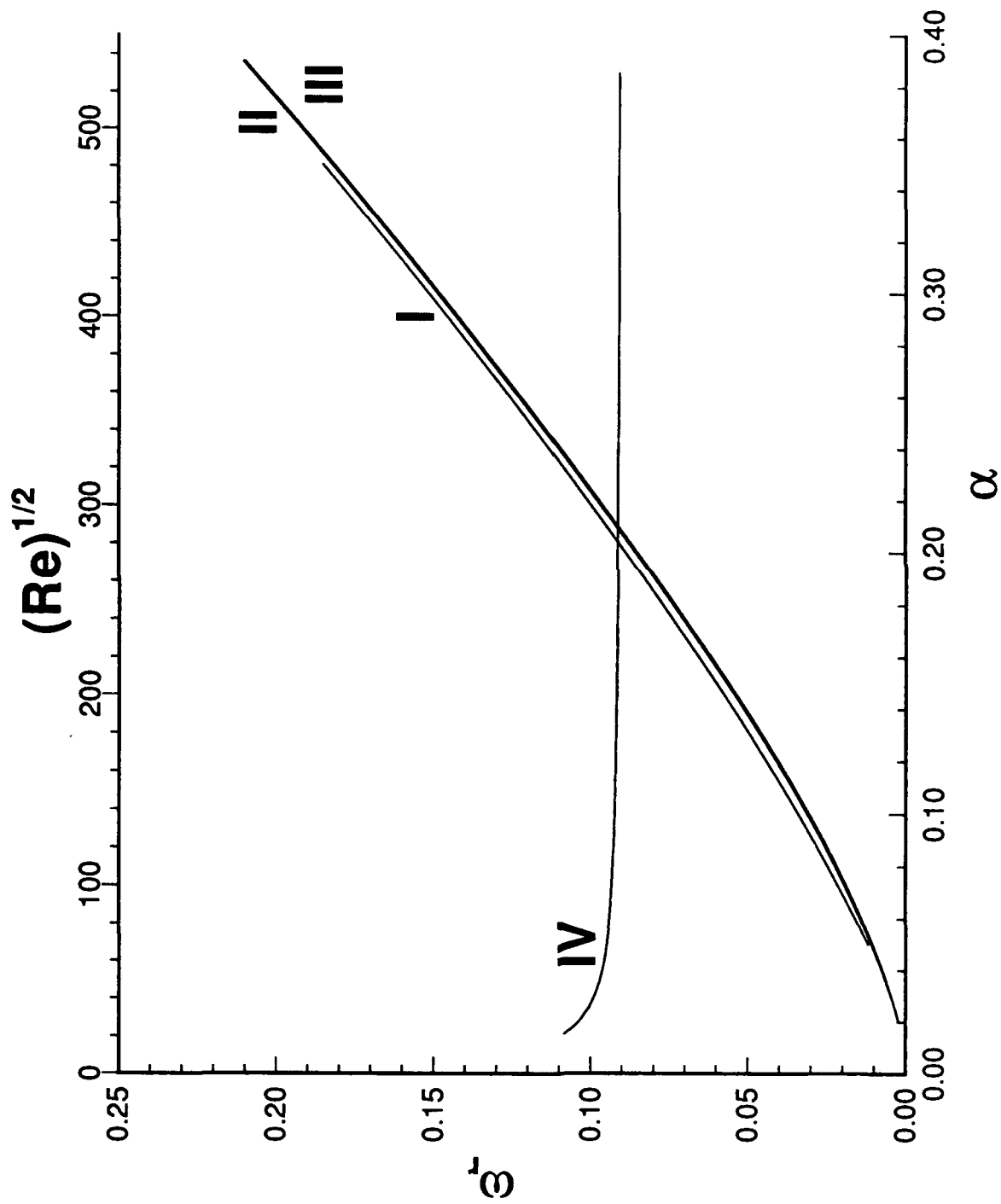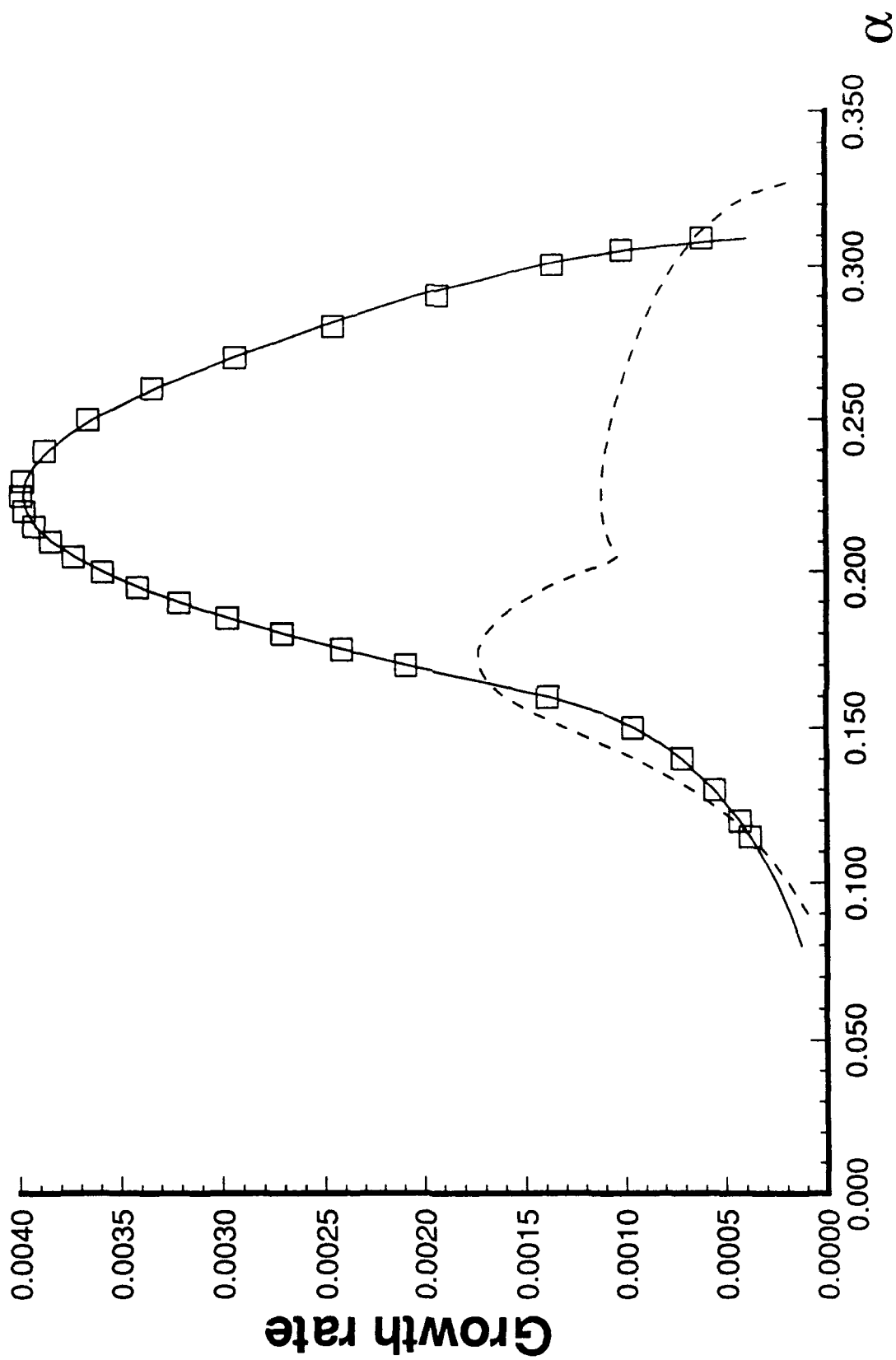
Figure 4

Figure 5

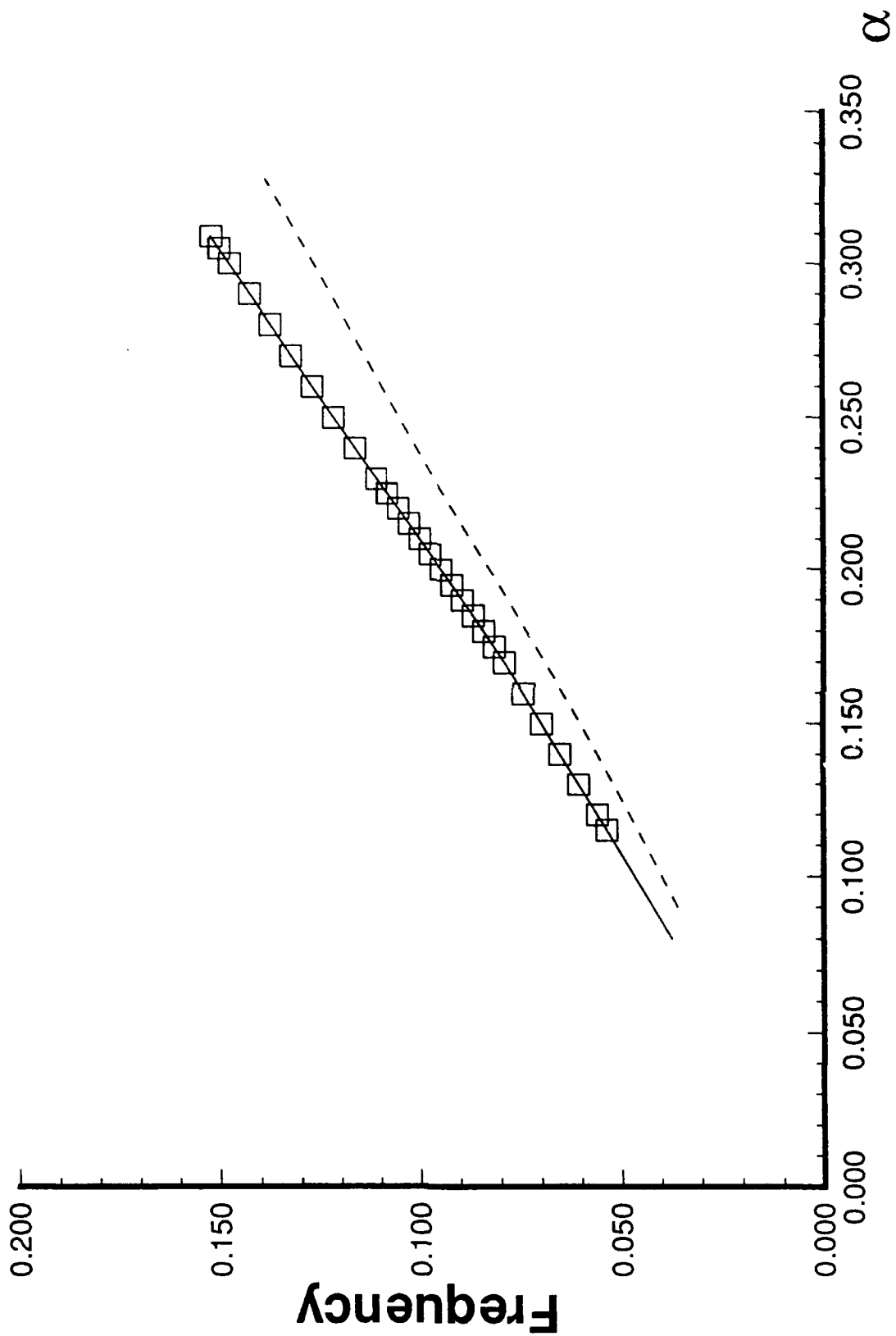**Figure 6**

Figure 7

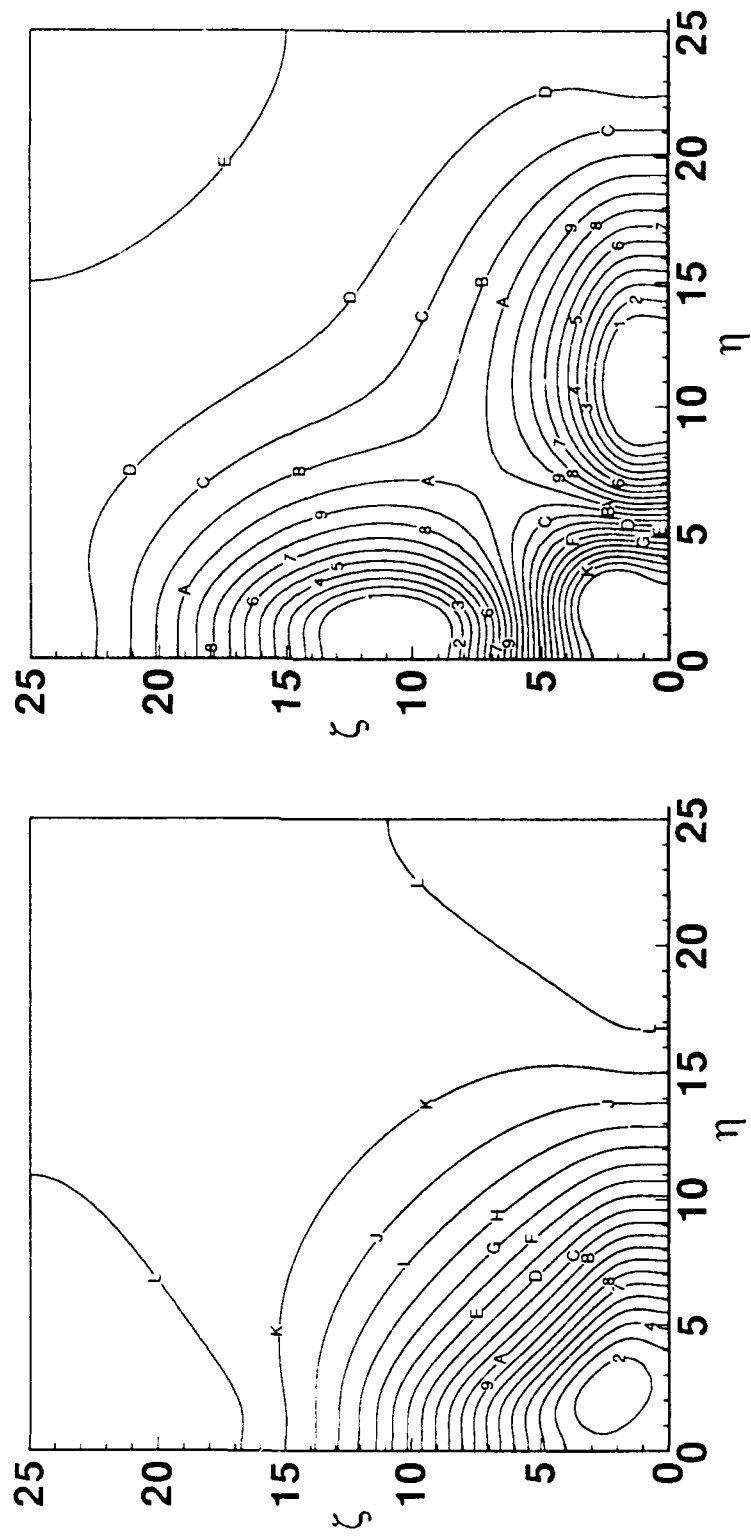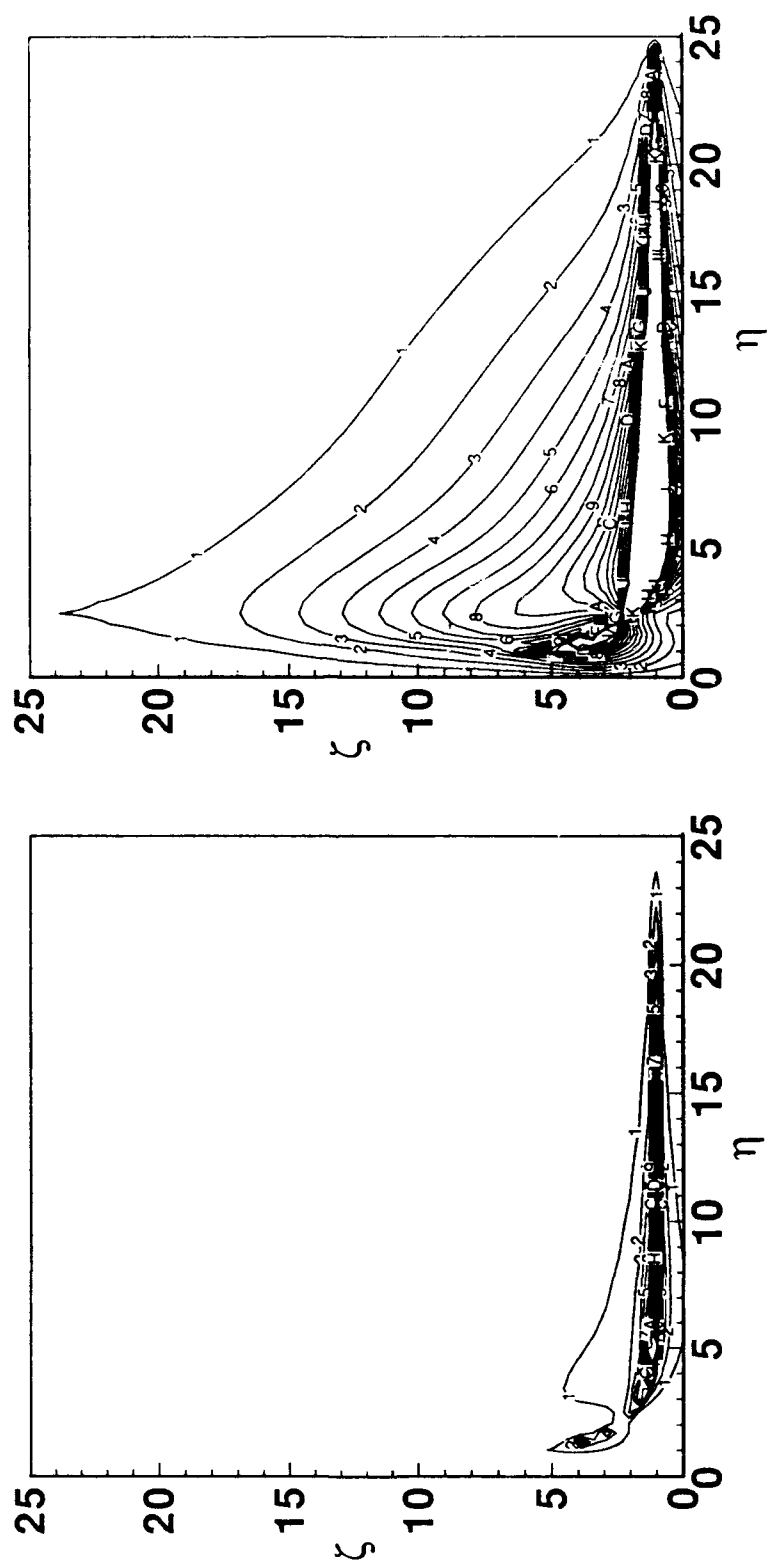**Figure 8**

Figure 9

21

REPORT DOCUMENTATION PAGE

Public reporting burden for this collection of information is estimated to average 1 hour per response including the time for reviewing instructions searching existing data sources gathering and maintaining the data needed, and completing and reviewing the collection of information. Send comments regarding this burden estimate or any other aspect of this collection of information, including suggestions for reducing this burden to Washington Headquarters Services, Directorate for Information Operations and Reports 1215 Jefferson Davis Highway, Suite 1204, Arlington, VA 22202-4302 and to the Office of Management and Budget, Paperwork Reduction Project (0704-0188) Washington, DC 20503

1. AGENCY USE ONLY (Leave blank)	2. REPORT DATE August 1993	3. REPORT TYPE AND DATES COVERED Contractor Report

4. TITLE AND SUBTITLE
INVISCID INSTABILITY OF STREAMWISE CORNER FLOW

5. FUNDING NUMBERS
C NAS1-19480

WU 505-90-52-01

6. AUTHOR(S)
S. Balachandar
M.R. Malik

7. PERFORMING ORGANIZATION NAME(S) AND ADDRESS(ES)
Institute for Computer Applications in Science
  and Engineering
Mail Stop 132C, NASA Langley Research Center
Hampton, VA 23681-0001

8. PERFORMING ORGANIZATION REPORT NUMBER
ICASE Report No. 93-54

9. SPONSORING/MONITORING AGENCY NAME(S) AND ADDRESS(ES)
National Aeronautics and Space Administration
Langley Research Center
Hampton, VA 23681-0001

10. SPONSORING/MONITORING AGENCY REPORT NUMBER
NASA CR-191514
ICASE Report No. 93-54

11. SUPPLEMENTARY NOTES
Langley Technical Monitor: Michael F. Card
Final Report

Submitted to Journal of
Fluid Mechanics

12a. DISTRIBUTION/AVAILABILITY STATEMENT
Unclassified - Unlimited

Subject Category 34

12b. DISTRIBUTION CODE

13. ABSTRACT (Maximum 200 words)
Linear stability of the incompressible flow along a streamwise corner is studied by solving the two-dimensional eigenvalue problem governed by partial differential equations. It is found that this fully three-dimensional flow is subject to inviscid instability due to the inflectional nature of the streamwise velocity profile. The higher growth rates for the inviscid instability mode, which is symmetric about the corner bisector, as compared to the viscous Tollmien-Schlichting instability operative away from the corner is consistent with the experimental findings that the corner flow transitions to turbulence earlier than the two-dimensional Blasius flow away from the corner.

14. SUBJECT TERMS
corner flow, inviscid, instability

15. NUMBER OF PAGES
25

16. PRICE CODE
A03

17. SECURITY CLASSIFICATION OF REPORT Unclassified	18. SECURITY CLASSIFICATION OF THIS PAGE Unclassified	19. SECURITY CLASSIFICATION OF ABSTRACT	20. LIMITATION OF ABSTRACT

☆U.S. GOVERNMENT PRINTING OFFICE: 1993 - 728-064/86068